Journal of Renewable Materials

Tech Science Press

DOI: 10.32604/jrm.2023.025112

ARTICLE

The Antibacterial Activities of Copper Oxide Nanoparticles Synthesized Using Laser Ablation in Different Surfactants against *Streptococcus mutans*

Ruaa H. Abbas[1], A. Kadhim[1,*] and Azhar M. Haleem[2]

[1]Laser and Optoelectronics Engineering Department, University of Technology-Iraq, Baghdad, Iraq

[2]Environmental Research Center, University of Technology-Iraq, Baghdad, Iraq

[*]Corresponding Author: A. Kadhim. Email: abdulhadikadhim5@gmail.com

Received: 22 June 2022 Accepted: 25 August 2022

ABSTRACT

Copper oxide nanoparticles (CuO NPs) were synthesised with laser ablation of a copper sheet immersed in deionized water (DW), cetrimonium bromide (CTAB), and sodium dodecyl sulphate (SDS), respectively. The target was irradiated with a pulsed Nd: YAG laser at 1064 nm, 600 mJ, a pulse duration of 10 ns, and a repetition rate of 5 Hz. The CuO NPs colloidal were analyzed using UV–Vis spectroscopy, the Fourier transform infrared (FTIR) spectrometer, zeta potential (ZP), X-ray diffraction (XRD), transmission electron microscope (TEM) and field emission scanning electron microscopy (FESEM). The absorption spectra of CuO NPs colloidal showed peaks at 214, 215 and 220 nm and low-intensity peaks at 645, 650 and 680 nm for SDS, CTAB and DW, respectively. CuO NPs' colloidal results are (−21.6, 1.2, and 80 mV) for negatively, neutrally, and positively charged SDS, DW, and CTAB, respectively. The XRD pattern of the NPs revealed the presence of CuO phase planes (110) (111), (20-2) and (11-1). The TEM images revealed nearly spherical NPs, with sizes ranging from 10–90, 10–50, and 10–210 nm for CuO NPs mixed with DW, SDS and CTAB, respectively. FESEM images of all the synthesized samples illustrate the formation of spherical nanostructure and large particles are observable. The CuO NPs were tested for antibacterial activity against *Streptococcus mutans* by using the well diffusion method. In this method, CuO NPs prepared in DW at a concentration of 200 μg/mL showed a greater inhibition zone against *Streptococcus mutans*.

KEYWORDS

Copper oxide nanoparticles (CuO NPs); laser ablation; *Streptococcus mutans*

1 Introduction

Antimicrobial compounds are used in a range of medical applications, including the protection of the environment, packaging, textiles, and medical equipment [1,2]. Nanotechnology has been proposed as a promising field of technology for a wide range of biomedical applications. Among the nanomaterials currently available, metal nanoparticles (MNPs) have been discovered as medicinal agent transporters [3]. NPs are being employed in the medical field as biopharmaceuticals, enzymes, DNA, and monoclonal antibodies. Until now, NPs have been polymeric and formed of metals and nonmetals. Materials and bioceramics [4]. Copper oxide nanoparticles (CuO NPs) have received a lot of interest among metal nanoparticles because of their nontoxicity, low cost, natural abundance, ease of manufacturing, and exceptional photovoltaic capabilities [5]. The prevalence of biological and bacterial infections has

increased in recent years, particularly in businesses that directly affect human consumption, such as food, food items, and water. This growing concern has prompted scientists to develop non-toxic, simple-to-use inorganic antibacterial nanoparticles. When certain materials, such as metal oxide semiconductors, are reduced to a tiny size, they can generate new materials with unique optical and electrical properties [6–8]. The technique of laser ablation in liquid has been used to produce a variety of nanoscale materials with a range of shapes and sizes that depend on the laser's strength, wavelength, and pulse duration [9]. Dental caries is an acute illness caused by harmful bacteria infecting the oral cavity [6]. *Streptococci* of the oral mucosa, particularly *S. mutans,* are the primary plaque-forming bacteria, by the activity of glucosyltransferase (GTFase) [7], they produce acid and insoluble glucan in water, which is the main source of oral bacteria or biofilm and the onset of tooth decay. Compared to other microbe groups, there are very few investigations into this bacteria's effect on metal-containing nanoparticles (NPs). However, this bacterium is clinically vital in dentistry [6–8]. Resistant bacteria are spreading worldwide, endangering antibiotic efficacy [9,10]. Smaller nanoparticles seem to penetrate bacteria better. In fact, interactions with membranes and any harm caused by these interactions are more apparent in nanoparticles with a positive zeta potential and a small diameter [11]. Zeta potentials were used as a tool to investigate the modification of bacterial cell surface permeability and maybe bacterial membrane penetration and subsequent bacterial viability [12–16].

2 Materials and Methods

2.1 Sample Preparation

As depicted in Fig. 1, a pure copper square plate 98% (with a thickness of 2 mm) was placed at the bottom of a glass jar containing 5 mL of DW, and DW was mixed with two aqueous solutions: 8 mM of CTAB and SDS surfactants, respectively. A copper target was focused using a 600 mJ Q-switched Nd: YAG laser (pulse duration = 10 ns, wavelength = 1064 nm, repetition rate = 5 Hz, and focal length = 10 cm). To quantify the nanoparticle concentration, the target sample was weighed before and after ablation using electronic weighing equipment.

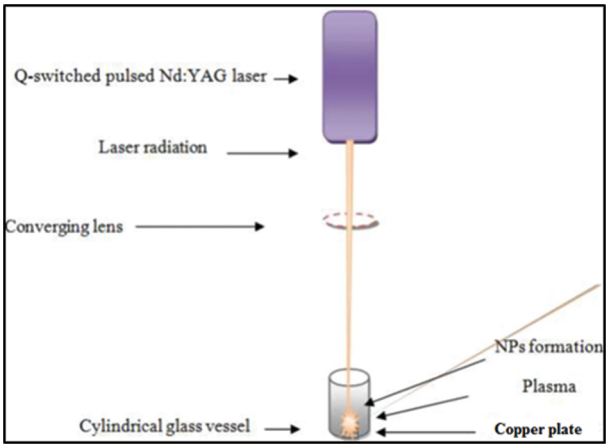

Figure 1: Schematic diagram of pulsed laser ablation

2.2 Characterization of CuO NPs

The prepared CuO NPs were characterised using optical, structural, and morphological techniques. A double beam UV-VIS spectrophotometer (Shimatzu SP8001) was used to measure the absorption spectrum of CuO NPs within the spectral range (200–800 nm). The Fourier transform infrared (FTIR) spectrometer type PerkinElmer spectrum two/USA was used to detect the chemical composition and functional groups of the prepared NPs. The Zeta potential was used to determine the surface charge of nanoparticles where it is a

measurement of the electrostatic or charge repulsion/attraction between particles. (XRD-6000 model, country of origin: Japan) It is used to measure the structural properties of NPs by dropping and drying the CuO NPs solution on an aluminium substrate radiation source at 2θ angle = (20°–80°)

$$D = 0.94\lambda/\beta COS\theta \quad (1)$$

where λ is the wavelength of X-ray (1.54060 Å), β is the full width at half maximum of diffraction θ is the diffraction angle [11]. The transmission electron microscope (TEM)-type (ZEDSS LEO 912 AB-100 KV) made in Germany was used to determine the size and morphological characterizations of CuO NPs. A drop of CuO NP solution was put onto a standard gold-coated copper grid for TEM sample preparation. The morphology and composition of CuO NPs were recorded by field emission scanning electron microscopy and energy dispersive X-ray spectroscopy, respectively (FESEM; ZEISS SIGMA VP/Germany).

2.3 Antibacterial Activity Assay

Streptococcus mutans was pre-activated by nutrient broth for 24 h at 37ºC to reach the exponential phase with a final number of 1×10^6 CFU/mL by McFarland solution before being inoculated on the solid surface of Muller Hinton agar using the well diffusion method for the antibacterial assay. Then, five wells with 6 mm diameters were created in agar, and 100 μL of nanoparticle solutions generated by laser ablation at various concentrations (0.0, 25, 50, 100, and 200 μg/mL) were added. Then all the plates were incubated at 37°C for 24 h. The inhibition zone around the wells was measured for 3 replicates, while the inhibition rate was calculated according to the following equation:

$$\text{inhibition rate}\% = (1 - x - \min)/(\max - \min) \times 100\% \quad (2)$$

Whereas X = colony diameter at any concentration

Min = least inhibition zone

Max = biggest inhibition zone

2.4 Estimation of Minimum Inhibition Concentration (MIC) and Minimum Bactericidal Concentration (MBC)

The Minimum Inhibition Concentration (MIC) of the prepared CuO NPs against *S. mutans* was measured by the serial dilution method (0.0, 25, 50, 100, and 200 μg/mL) in Mueller–Hinton broth. All tubes were pre-inoculated with 10 μL of 1×10^6 CFU/mL of tested bacteria. All inoculated tubes were incubated for 24 h at 37°C. The lowest concentration with no visual turbidity was regarded as the MIC. The MBC of CuO NPs has been estimated by taking 100 μL from MIC tubes that have not given any visual turbidity and inoculating them on Mueller–Hinton surface agar and keeping them at 37°C for 24 h after the incubation period, the lowest dilution that gave no single colony of growth bacteria considered as MBC.

2.5 Statistical Analysis

All data were statistically analyzed using ANOVA test to express the significant differences at ($P < 0.05$) by using least significant differences (LSD).

3 Results and Discussion

3.1 UV–vis Absorption Investigation

Using a UV-vis absorption spectrophotometer (Shimatzu SP8001), the optical characteristics of the colloidal were determined. When the laser pulse struck the immersed target, a cloud formed on the object's surface. After the surface layer absorbed the laser pulses, a dense plasma was created. Increasing the solvent density and viscosity restricted the plasma closer to the copper plate surface during laser ablation of a Cu target. For example, high-pressure shockwaves generated by confined plasma could etch the surface of the metal plate, causing secondary ablation [17,18]. The absorption spectra of CuO NPs have an absorption peak near 215 nm and a low-intensity peak near 650 nm. The rise in peak intensity in

all NP-containing solutions with surfactants over deionised water implies an increase in CuO NPs production efficiency [18,19]. The density and viscosity of water were lower than those of other solutions, including surfactants. CuO NPs could be generated in a melting process using deionised water. As a result, the plasma plume's temperature, pressure, and density were reduced. The production efficiency of CuO NPs in SDS was higher than in CTAB as shown in Fig. 2, where surfactants increase solvent density and viscosity, restricting the plasma at the Cu target's surface, which increases CuO NPs production efficiency. The high pressure of the confined plasma at the copper plate's surface could etch it via a secondary ablation process triggered by high-pressure shockwaves, generating additional nanoparticles [19].

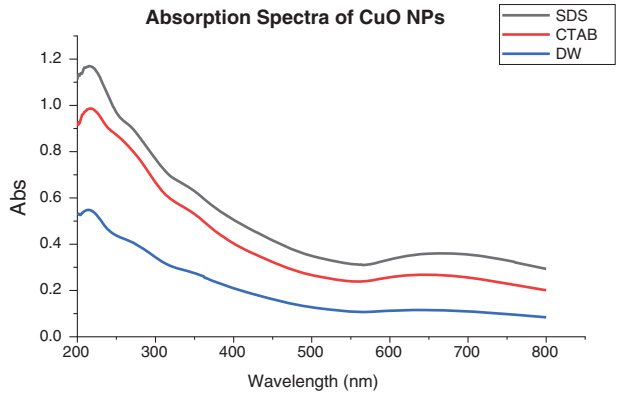

Figure 2: Absorption spectra of CuO NPs

3.2 FTIR

FTIR is used to determine the nature of bonding vibrations, provides significant information on chemical bonding within a substance and to examine the adsorption of surfactants onto the surface of CuO NPs [20–24]. The IR spectra of CuO, CuO-SDS, and CuO-CTAB samples are shown in Fig. 3. The presence of copper oxide in a monoclinic structure is shown by the vibration bands at 555 and 594 cm^{-1} and attributed to Cu-O vibrations, verifying the synthesis of CuO NPs [20,21]. The presence of CO_2 adsorbed on the samples' external surface and the existence of C-H stretching vibration of methyl and methylene groups of CTAB are responsible for the broad absorption bands at nearly 2137 cm^{-1}. The broad absorption peak at 3332 cm^{-1} is due to the stretching frequency of absorbed water's-OH group because nanocrystalline materials have a high surface-to-volume ratio and absorb moisture. The appearance of a small peak at 1010 cm^{-1} is attributed to the anionic surfactant molecules where the S=O stretching vibration of SO_4 from SDS [22,23]. Furthermore, the band around 1631 cm^{-1} can be attributed to carboxyl groups and could be hydroxyls (O-H) bending with copper atoms [20,24,25].

3.3 Zeta Potential

As shown in Fig. 4, the zeta potential (ZP) peak distribution results are −21.6, 1.2, and 80 mV for negatively, neutrally, and positively charged SDS, DW, and CTAB, respectively. The zeta potential is an important characterization approach of nanocrystals to determine surface charge, which can be used to evaluate nanosuspension physical stability. High ZP particles are highly charged, preventing particle aggregation due to electrostatic repulsion. If the ZP is low, attraction wins over repulsion, and the mixture coagulates [26]. Other factors affecting the physical stability of produced nanosuspensions include material characteristics, surfactant presence, and solution chemistry. The surface coverage of anionic surfactants such as SDS increased when they fully covered the positively charged surface of nanoparticles, reducing re-aggregation. Using anionic surfactants, SDS may generate multiple layers of surfactants on NP surfaces, whereas CTAB cannot, so the particle surfaces were charged and thoroughly covered with SDS surfactant [27].

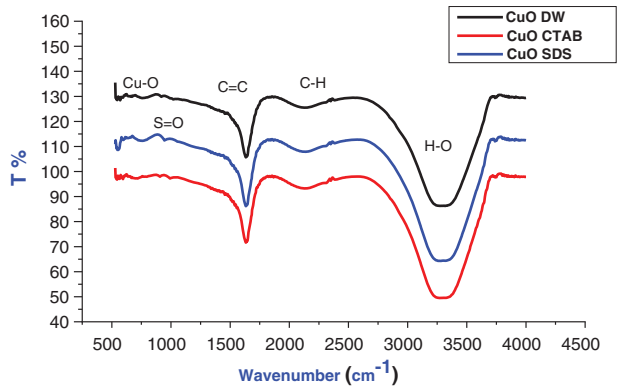

Figure 3: FTIR of CuO NPs with different solutions

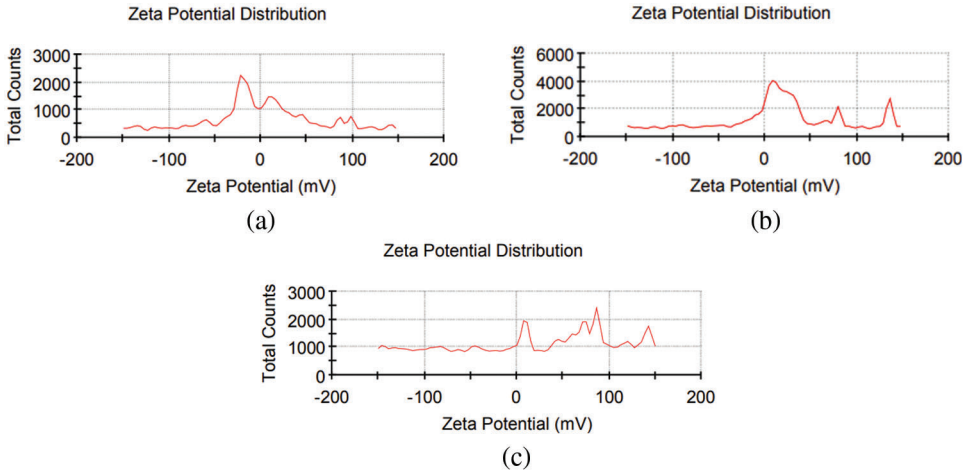

Figure 4: Zeta potential of CuO NPs colloidal with (a) SDS, (b) DW, and (c) CTAB

3.4 Structural Properties

The phase structure of CuO NPs was investigated using XRD. All of the reflections were well correlated with the monoclinic crystal phase of the copper oxide structure, and matched phase standard values of the plane of CuO crystal according to Card No. 96-900-8962, as illustrated in Fig. 5. Table 1 contains a list of all the XRD parameters of CuO NPs. The amazing crystallinity can be attributed to the sharpness and number of peaks in the XRD pattern. The crystalline size of NPs (C.s) was determined using the Scherrer formula. The following Table 1 summarises the XRD results for experimental CuO NPs, including the peak position 2, crystalline size variation, full width half maximum (FWHM), and interplanar spacing (dhkl) and miller index (hkl).

3.5 Morphologies of CuO NPs

3.5.1 TEM Imaging

The particle size distribution and morphological properties of CuO NPs were studied using TEM. The TEM image and particle size distribution of CuO NPs generated in a DW environment are demonstrated in Figs. 6a and 6b, where the TEM image indicates that a spherical graphitic shape of CuO NPs with a particle size distribution ranged between 10 and 90 nm were observed, and the majority of NPs are near to each other, resulting in a chain-like pattern. Previous research has shown that laser ablation synthesis of metal NPs in DW results in NPs with constant aggregation [28]. Figs. 6c and 6d show TEM visualisation and a narrow

size distribution of nanoparticles (10–50 nm). The size of nanoparticles generated in SDS surfactant was determined by the competition between successive particle growth and SDS coating. Thus, raising the SDS concentration may improve the protection of Cu particles by SDS molecules against diffusion-based incorporation of Cu atoms. Consequently, the particle surfaces were completely coated with SDS surfactant molecules, preventing further development due to surface charges [29]. Figs. 6e and 6f demonstrate that spherical, nonhomogeneous, and non-agglomerated CuO NPs were generated at CTAB colloidal (20 to 200 nm). CuO NPs prepared in SDS have a smaller average size than those prepared in CTAB. The proportion of smaller nanoparticles generated by nanosecond pulsed laser ablation in SDS solution was higher than in CTAB solution, which was attributable to the stability of the nanoparticles' solution. The longer tail of the CTAB surfactant and the extensive surface coverage attained by the SDS surfactants may explain the larger NP size produced by CTAB. The SDS solution inhibited NPs growth more than the CTAB solution [30].

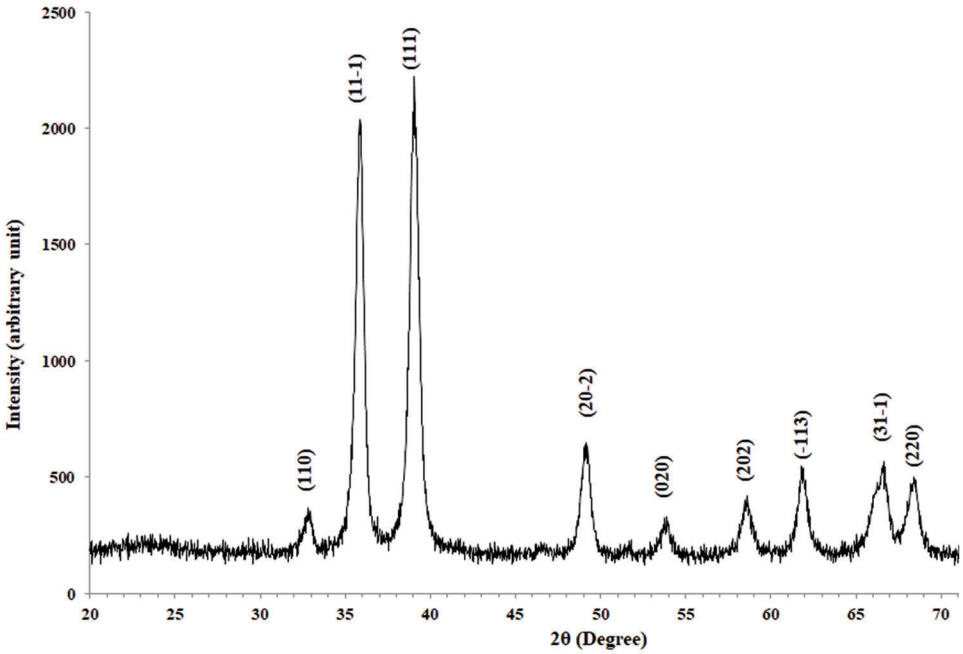

Figure 5: XRD of CuO NPs

Table 1: XRD of CuO NPs

2θ (Deg.)	FWHM (Deg.)	d_{hkl} Exp. (Å)	G.S (nm)	hkl	d_{hkl} Std. (Å)	Card No.
35.86	0.574	2.50	14.6	(11-1)	2.51	96-900-8962
32.81	0.604	2.73	13.7	(110)	2.73	96-900-8962
39.06	0.635	2.30	13.3	(111)	2.31	96-900-8962
53.86	0.54	1.70	16.4	(020)	1.71	96-900-8962
49.18	0.69	1.85	12.6	(20-2)	1.85	96-900-8962
58.58	0.665	1.57	13.7	(202)	1.57	96-900-8962
68.43	0.69	1.37	13.8	(220)	1.36	96-900-8962
66.62	0.755	1.40	12.6	(31-1)	1.40	96-900-8962
61.81	0.604	1.49	15.3	(−113)	1.48	96-900-8962

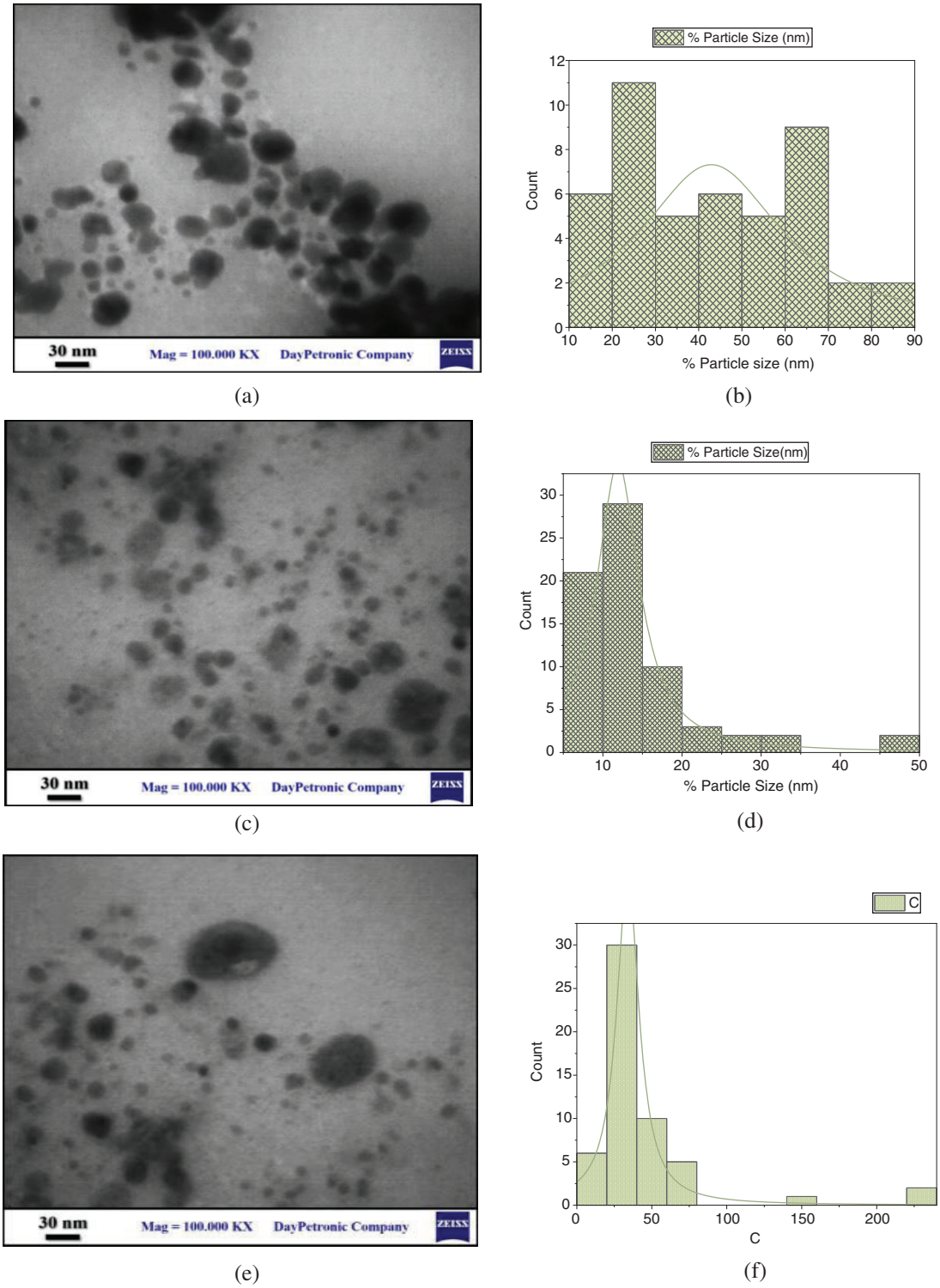

Figure 6: (a) morphological properties of CuO NPs synthesized with DW, (b) particle size distribution, (c) morphological properties of CuO NPs synthesized with SDS, (d) particle size distribution. (e) morphological properties of CuO NPs synthesized with CTAB, and (f) particle size distribution

3.5.2 FESEM Imaging

As shown in Figs. 7–9, several FESEM images of CuO NPs prepared in different solutions (DW, SDS, and CTAB) were captured to perform morphology of CuO NPs, where drops of each colloidal sample were dried on quartz slides. Due to the nanoparticle production method, large particles are observable on the samples. This is a typical outcome of laser ablation. When high-intensity laser pulses contact a copper target, the interaction zone's temperature rises to its boiling point, causing an explosion in which nanodroplets (clusters of free atoms) are blasted from the target onto the substrate surface. These nanodroplets can solidify on the substrate and form spherical micrometric and submicrometric particles, which seem to be formed as a result of fine nanoparticle aggregation while ionized matter nucleates and grows [31,32]. The EDS examination indicates that even the micrometric particles are copper or copper oxide, as shown in Figs. 7–9. Furthermore, some agglomerated nanoparticles were observed in DW while the strong interaction between SDS/CTAB and Cu ion prevented copper atoms from aggregating into larger particles. This is a common effect of laser ablation due to the mechanism of nanoparticle creation [33]. It is clear in the FESEM images that the morphology of laser ablated nanostructures is spherical in shape and does not change significantly with changing liquid media such as SDS and CTAB, and the size of CuO nanospheres is slightly decreased with ablation in the SDS surfactant and increased in CTAB. This prompted the use of SDS and CTAB surfactants as nanoparticle stabilizing agents, which protect them from aggregation and other external influences [34].

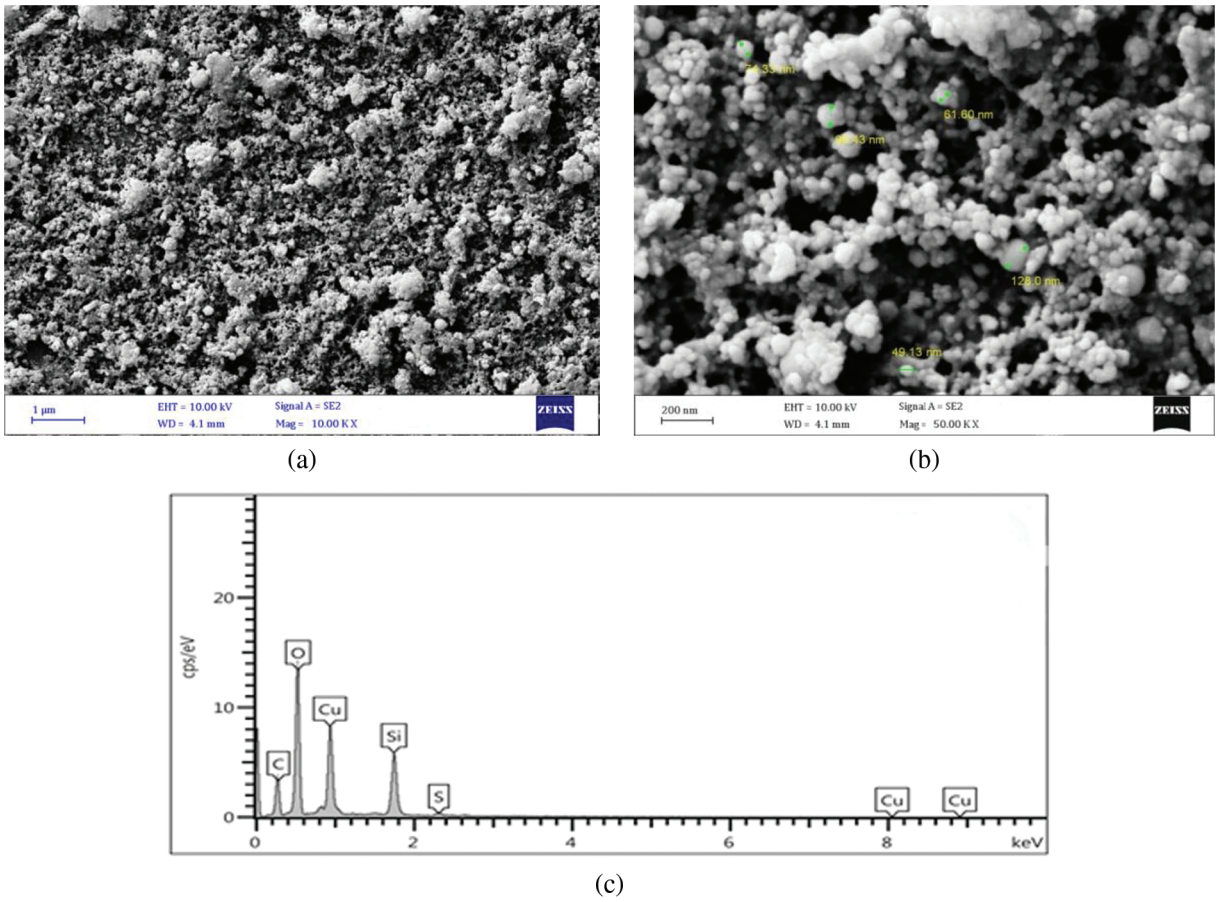

Figure 7: FESEM images of CuO NPs synthesied in DW (a) FESEM at mag = 10.00 KX, (b) FESEM at mag = 50.00 KX, and (c) EDS

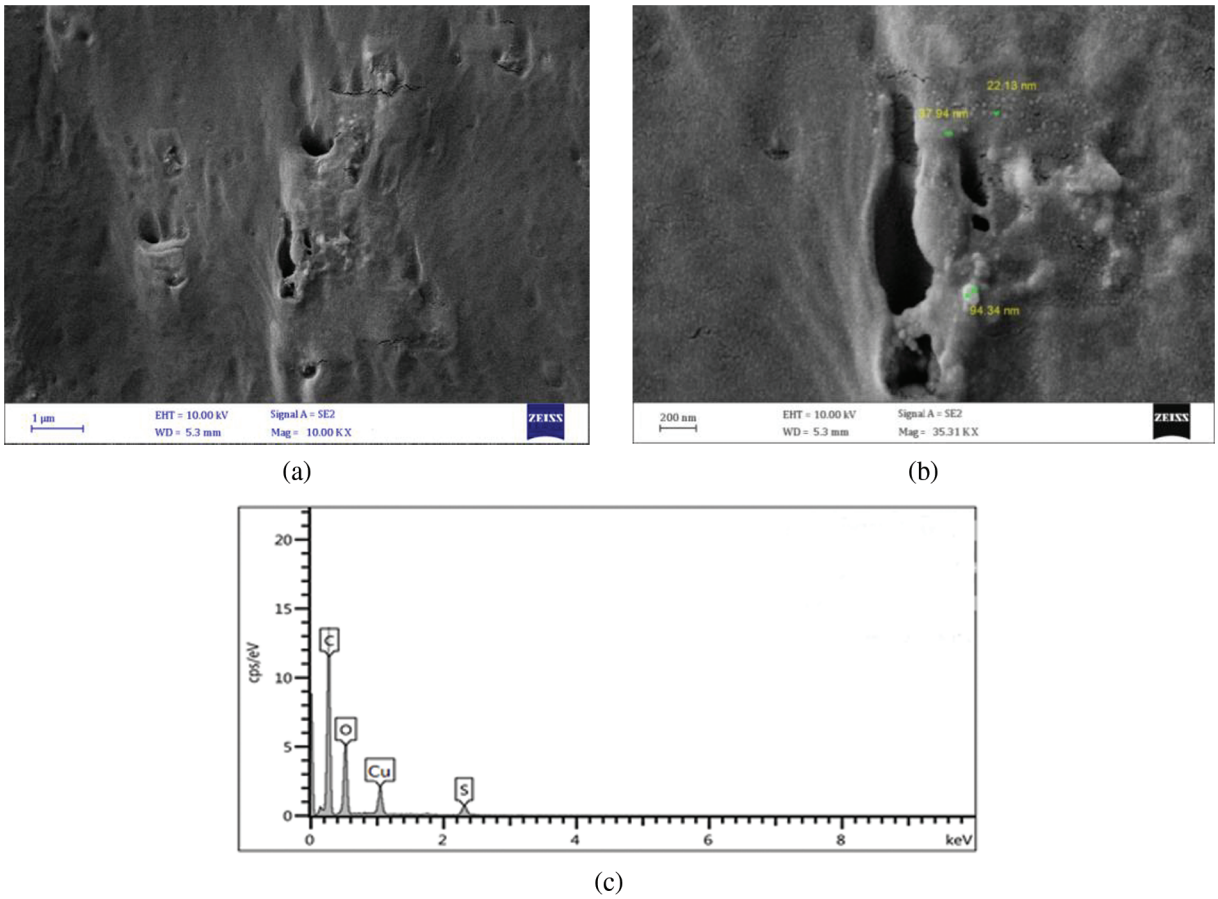

Figure 8: FESEM images of CuO NPs synthesied in SDS (a) FESEM at mag = 10.00 KX, (b) FESEM at mag = 35.31 KX, and (c) EDS

3.6 Antibacterial Assay

The antibacterial efficacy of CuO NPs against *Streptococcus mutans* was examined. The well diffusion method was utilized to identify the presence of an inhibitory zone in order to evaluate the antibacterial ability of different nanoparticle concentrations. CuO NPs improved antibacterial activity where the inhibition zone diameters increased with CuO NPs concentrations (0.0, 25, 50, 100, and 200 µg/mL). As the concentration of CuO NPs increases, so does its antibacterial activity. As shown in Figs. 10–13, where inhibition rate of *Streptococcus mutans* and inhibition zone of colony diameters increase with CuO NPs concentrations, it can be observed that there can be statistically significant differences in concentrations of CuO NPs and the materials used in preparing the nanoparticles (DW, SDS, and CTAB) because the *p* value was less than 0.05, where the higher concentration of CuO NPs prepared in DW being more effective as an antibacterial agent. Numerous sulfur-containing proteins line bacterial cell membranes, making them susceptible to silver nanoparticles' reactions with sulfur-containing amino acids on both sides of the membrane. The Cu ions produced by CuO NPs have been hypothesised to connect with phosphorus moieties in DNA, blocking DNA replication, or to react with sulfur-containing proteins, blocking enzyme functions and affecting cell viability and, ultimately, cell death. Uncertainty remains as to whether a single mechanism or a mix of processes caused the death. One of these may be attributable to the interaction of AgNPs with the bacterial cell wall and the simultaneous entry of Ag ions into bacterial cells. Electrostatic interaction between positively charged NPs and negatively charged bacterial cell

surfaces is crucial for NPs' activity as a bactericidal agent and is responsible for much of the antibacterial activity of NPs in general. The current study, like earlier studies, shows that NPs lead to mitochondrial and DNA damage, resulting in cell death. This is because mitochondrial damage and the upregulation of the expression of many apoptotic proteins are the causes of cell death [35,36]. CuO NPs can cause oxidative stress, heterogeneous changes, and abnormalities in cellular uptake, electrolyte imbalances, and protein deactivation when they interact with DNA, lysosomes, ribosomes, and enzymes. NPs can also cause gene expression and enzyme inactivation [37,38]. Metallic nanoparticles (MNs) and their accompanying ions produce superoxide radicals (ROS), which cause oxidative stress in cells. Metallic nanoparticle dissolution and attachment on bacterial membranes, resulting in membrane rupture and dissipation of the protein motivational force, enhanced permeability [39]. Nanotechnology was also used in orthodontic brackets and wires/ligatures. Biofilms tend to collect on micro-implants and orthodontic retainers. CuO NPs and (CuO-ZnO) NPs displayed better antibacterial effects than ZnO NPs. *In vivo*, orthodontic retainers with AgNPs demonstrated a substantial antibacterial effect against *S. mutans* during deboning. Due to NPs' cellular toxicity and rising evidence of their potentially harmful effects, caution should be exercised in their widespread use [40,41].

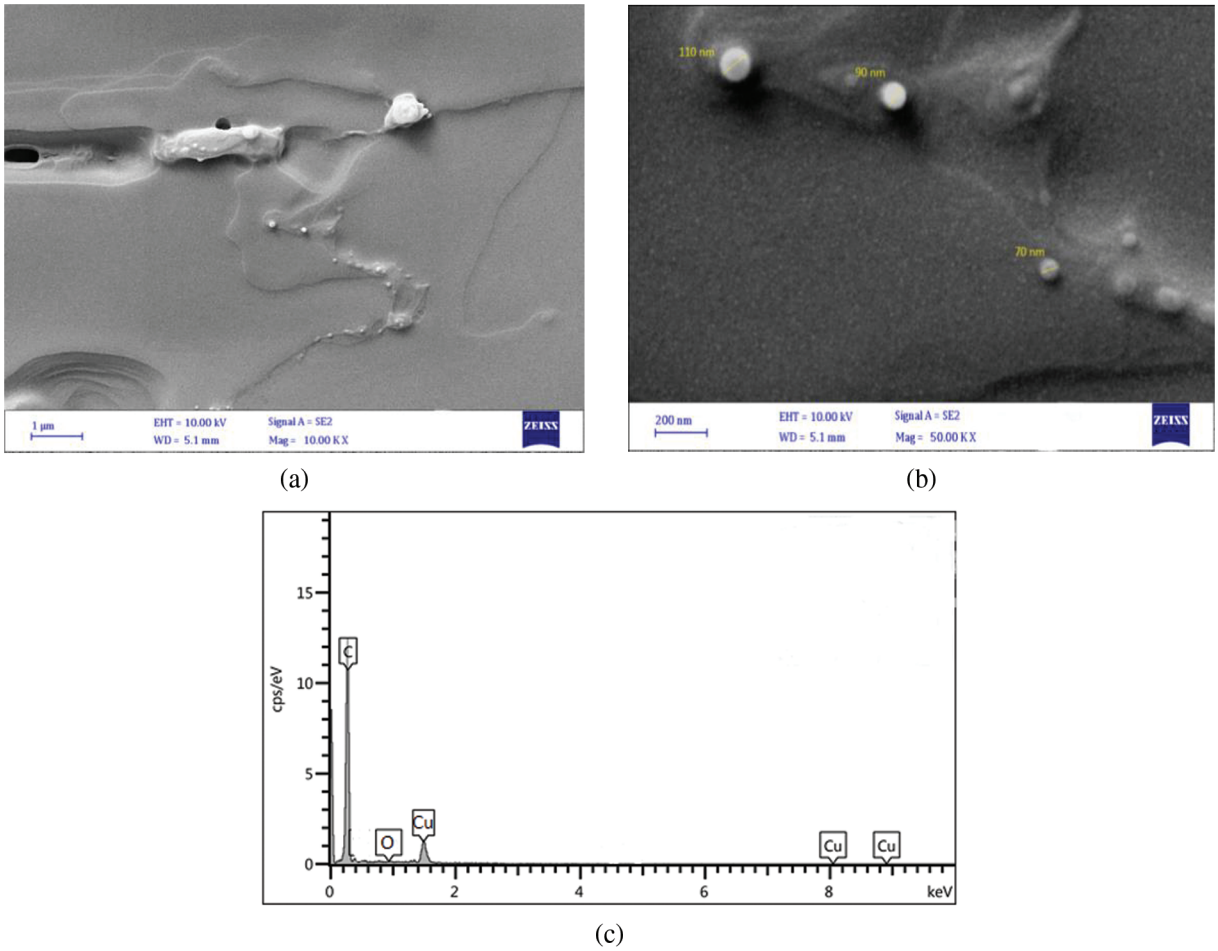

Figure 9: FESEM images of CuO NPs synthesied in CTAB (a) FESEM at mag = 10.00 KX, (b) FESEM at mag = 50.00 KX, and (c) EDS

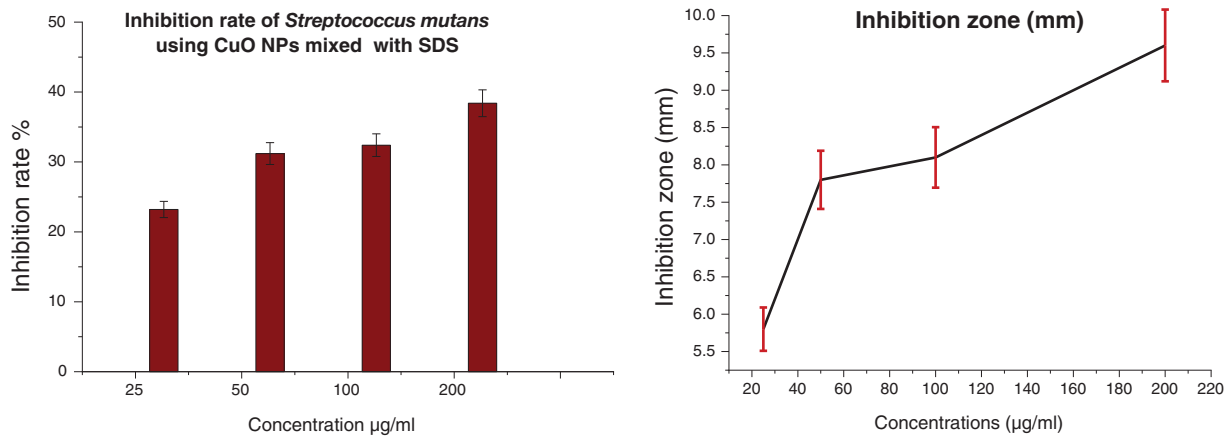

(a) (b)

Figure 10: (a) Inhibition rate (%) of *Streptococcus mutans* treated with CuO NPs synthesized with SDS, and (b) Inhibition zone (mm) of *Streptococcus mutans* treated with CuO NPs

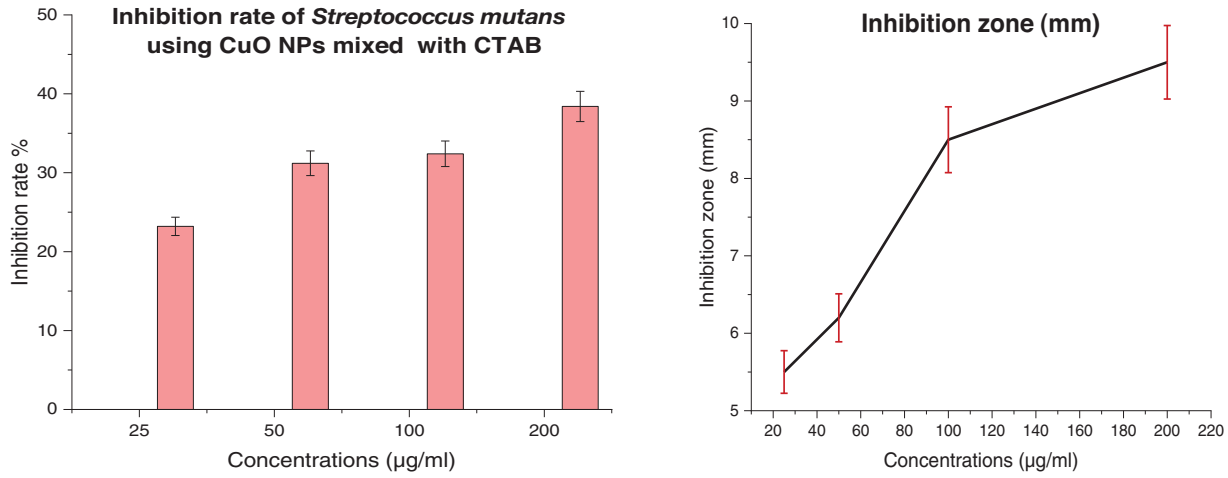

(a) (b)

Figure 11: (a) Inhibition rate (%) of *Streptococcus mutans* treated with CuO NPs with CTAB, and (b) Inhibition zone (mm) of *Streptococcus mutans* treated with CuO NPs with CTAB

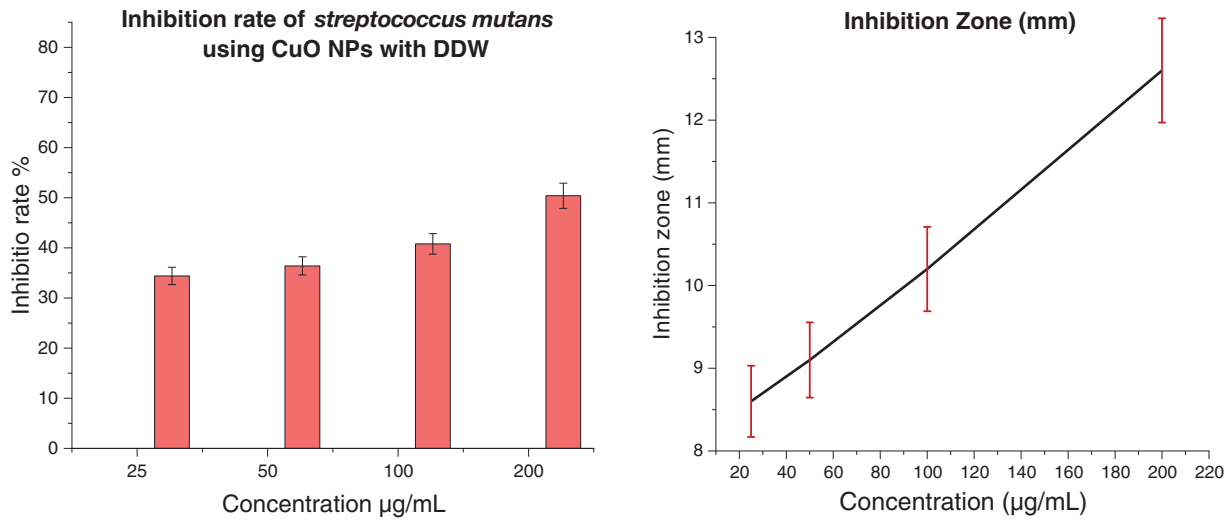

(a) (b)

Figure 12: (a) Inhibition rate (%) of *Streptococcus mutans* treated with CuO NPs with DW, and (b) Inhibition zone (mm) of *Streptococcus mutans* treated with CuO NPs with DW

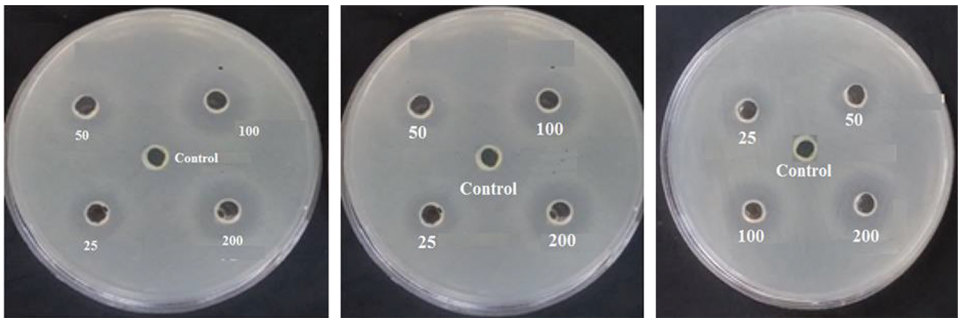

(a) (b) (c)

Figure 13: The inhibition zone (mm) of prepared CuO NPs on *Streptococcus mutans* (a) DW, (b) SDS, and (c) CTAB

4 Conclusion

The results demonstrated that ablation with a Q-switched Nd: YAG laser is capable of preparing CuO NPs with nearly 215 and 650 nm absorption spectra for CuO NPs ablated in DW, SDS, and CTAB, respectively. Ablation in DW, SDS, and CTAB liquids results in spherical particles of CuO NPs, with a smaller particle size of SDS than CTAB. An *in vitro* assay showed that prepared CuO NPs have significant antibacterial activity against *Streptococcus mutans*.

Funding Statement: The authors received no specific funding for this study.

Conflicts of Interest: The authors declare that they have no conflicts of interest to report regarding the present study.

References

1. Kenawy, E. R., Worley, S. D., Broughton, R. (2007). The chemistry and applications of antimicrobial polymers: A state-of-the-art review. *Biomacromolecules, 8(5),* 1359–1384. DOI 10.1021/bm061150q.
2. Karim, N., Afroj, S., Lloyd, K., Oaten, L. C., Andreeva, D. V. et al. (2020). Sustainable personal protective clothing for healthcare applications: A review. *ACS Nano, 14(10),* 12313–12340. DOI 10.1021/acsnano.0c05537.
3. Lianga, S. X. T., Wong, L. S., Lim, Y. M., Djearamanea, S., Lee, P. F. (2020). Effects of Zinc oxide nanoparticles on Streptococcus pyogenes. *South African Journal of Chemical Engineering, 34(1),* 63–71. DOI 10.1016/j.sajce.2020.05.009.
4. Bahadar, H., Maqbool, F., Niaz, K., Abdollahi, M. (2016). Toxicity of nanoparticles and an overview of current experimental models. *Iranian Biomedical Journal, 20(1),* 1.
5. Menazea, A. A., Ahmed, M. K. (2020). Synthesis and antibacterial activity of graphene oxide decorated by silver and copper oxide nanoparticles. *Journal of Molecular Structure, 1218,* 128536. DOI 10.1016/j.molstruc.2020.128536.
6. Asawahame, C., Sutjarittangtham, K., Eitssayeam, S., Tragoolpua, Y., Sirithunyalug, B. et al. (2015). Antibacterial activity and inhibition of adherence of *Streptococcus mutans* by propolis electrospun fibers. *AAPS Pharmscitech, 16(1),* 182–191. DOI 10.1208/s12249-014-0209-5.
7. Haleem, A. M., Abbas, R. H., Jawad, M. A., Alberaqdar, F. (2019). Cytotoxic effects of titanium dioxide nanaoparticles synthesized by laser technique on peripheral blood lymphocytes and hep-2 cell line. *Toxicology and Environmental Health Sciences, 11(3),* 219–225. DOI 10.1007/s13530-019-0407-3.
8. Besinis, A., de Peralta, T., Handy, R. D. (2014). The antibacterial effects of silver, titanium dioxide and silica dioxide nanoparticles compared to the dental disinfectant chlorhexidine on *Streptococcus mutans* using a suite of bioassays. *Nanotoxicology, 8(1),* 1–16. DOI 10.3109/17435390.2012.742935.
9. Sánchez-López, E., Gomes, D., Esteruelas, G., Bonilla, L., Lopez-Machado, A. L. et al. (2020). Metal-based nanoparticles as antimicrobial agents: An overview. *Nanomaterials, 10(2),* 292. DOI 10.3390/nano10020292.
10. Abass, R. H., Haleem, A. M., Hamid, M. K., Kadhim, A., Jawad, R. S. (2017). Antimicrobial activity of TiO_2 NPs against *Escherichia coli* ATCC 25922 and *Staphylococcus aureus* ATCC 25923. *International Journal of Computation and Applied Sciences, 2(1),* 6–10.
11. Haleem, A. M., Kadhim, A., Abbas, R. H. (2017). Antibacterial activity of copper oxide nanoparticles against *Escherichia coli* ATCC 25922 and *Staphylococcus aureus* ATCC 25923. *Advances in Natural and Applied Sciences, 11(3),* 1–6.
12. Franci, G., Falanga, A., Galdiero, S., Palomba, L., Rai, M. et al. (2015). Silver nanoparticles as potential antibacterial agents. *Molecules, 20(5),* 8856–8874. DOI 10.3390/molecules20058856.
13. Gao, F., Pang, H., Xu, S., Lu, Q. (2009). Copper-based nanostructures: Promising antibacterial agents and photocatalysts. *Chemical Communications, (24),* 3571–3573. DOI 10.1039/b904801d.
14. Khashan, K. S., Sulaiman, G. M., Hamad, A. H., Abdulameer, F. A., Hadi, A. (2017). Generation of NiO nanoparticles via pulsed laser ablation in deionised water and their antibacterial activity. *Applied Physics A, 123(3),* 1–10. DOI 10.1007/s00339-017-0826-4.
15. Haleem, A. M., Khaleel, H. K. (2020). Histopathological and cytogenetic effects of copper oxide nanoparticles in the mice after oral administration. *Biochemical and Cellular Archives, 20(2),* 6259–6265.
16. Kadhim, A., Haleem, A. M., Abass, R. H. (2016). Anti-dermatophyte activity of Ti [O. sub. 2] NPs colloidal prepared by pulsed laser ablation in liquid environment. *Advances in Environmental Biology, 10(12),* 43–55.
17. Chaichan, M. T., Al-Asadi, K. A. (2015). Environmental impact assessment of traffic in Oman. *International Journal of Scientific & Engineering Research, 6(7),* 493–496.
18. Kazem, H. A., Chaichan, M. T. (2015). Effect of humidity on photovoltaic performance based on experimental study. *International Journal of Applied Engineering Research, 10(23),* 43572–43577.
19. Tsuji, T., Thang, D. H., Okazaki, Y., Nakanishi, M., Tsuboi, Y. et al. (2008). Preparation of silver nanoparticles by laser ablation in polyvinylpyrrolidone solutions. *Applied Surface Science, 254(16),* 5224–5230. DOI 10.1016/j.apsusc.2008.02.048.

20. Arakha, M., Saleem, M., Mallick, B. C., Jha, S. (2015). The effects of interfacial potential on antimicrobial propensity of ZnO nanoparticle. *Scientific Reports, 5(1),* 1–10. DOI 10.1038/srep09578.
21. Quirino, M. R., Lucena, G. L., Medeiros, J. A., Santos, I. M. G. D., Oliveira, M. J. C. D. (2018). CuO rapid synthesis with different morphologies by the microwave hydrothermal method. *Materials Research, 21*. DOI 10.1590/1980-5373-mr-2018-0227.
22. Dubal, D. P., Dhawale, D. S., Salunkhe, R. R., Jamdade, V. S., Lokhande, C. D. (2010). Fabrication of copper oxide multilayer nanosheets for supercapacitor application. *Journal of Alloys and Compounds, 492(1–2),* 26–30. DOI 10.1016/j.jallcom.2009.11.149.
23. Benhadria, N., Hachemaoui, M., Zaoui, F., Mokhtar, A., Boukreris, S. et al. (2022). Catalytic reduction of methylene blue dye by copper oxide nanoparticles. *Journal of Cluster Science, 33(1),* 249–260. DOI 10.1007/s10876-020-01950-0.
24. Ramimoghadam, D., Hussein, M. Z. B., Taufiq-Yap, Y. H. (2012). The effect of sodium dodecyl sulfate (SDS) and cetyltrimethylammonium bromide (CTAB) on the properties of ZnO synthesized by hydrothermal method. *International Journal of Molecular Sciences, 13(10),* 13275–13293. DOI 10.3390/ijms131013275.
25. Su, G., Yang, C., Zhu, J. J. (2015). Fabrication of gold nanorods with tunable longitudinal surface plasmon resonance peaks by reductive dopamine. *Langmuir, 31(2),* 817–823. DOI 10.1021/la504041f.
26. Hafizah, M. A. E., Riyadi, A. F., Manaf, A. (2019). Particle size reduction of polyaniline assisted by anionic emulsifier of sodium dodecyl sulphate (SDS) through emulsion polymerization. *IOP Conference Series: Materials Science and Engineering, 515(1),* 012080. DOI 10.1088/1757-899X/515/1/012080.
27. Thajeel, A. A., Ibrahem, M. A., Ahmed, D. S. (2022). Nanoplasmonic sensing using gold nanostructures. *Journal of Applied Sciences and Nanotechnology, 2(2),* 8–15. DOI 10.53293/jasn.2021.4282.1087.
28. Chen, Y. H., Yeh, C. S. (2002). Laser ablation method: Use of surfactants to form the dispersed Ag nanoparticles. *Colloids and Surfaces A: Physicochemical and Engineering Aspects, 197(1–3),* 133–139. DOI 10.1016/S0927-7757(01)00854-8.
29. Hamad, A., Li, L., Liu, Z. (2015). A comparison of the characteristics of nanosecond, picosecond and femtosecond lasers generated Ag, TiO_2 and Au nanoparticles in deionised water. *Applied Physics A, 120(4),* 1247–1260. DOI 10.1007/s00339-015-9326-6.
30. Mafuné, F., Kohno, J. Y., Takeda, Y., Kondow, T., Sawabe, H. (2000). Structure and stability of silver nanoparticles in aqueous solution produced by laser ablation. *The Journal of Physical Chemistry B, 104(35),* 8333–8337. DOI 10.1021/jp001803b.
31. Sabeeh, S. H., Hussein, H. A., Judran, H. K. (2016). Synthesis of a complex nanostructure of CuO via a coupled chemical route. *Materials Research Express, 3(12),* 125025. DOI 10.1088/2053-1591/3/12/125025.
32. Pavithra, K. S., Yashoda, M. P., Prasannakumar, S. (2019). Synthesis, characterisation and thermal conductivity of CuO-water based nanofluids with different dispersants. *Particulate Science and Technology, 38(5),* 559–567.
33. Ali, A. K. et al. (2021). Preparation of blue luminescence gold quantum dots using laser ablation in aromatic solvents. *Applied Nanoscience, 11(12),* 2779–2791.
34. Azadi, H., Aghdam, H. D., Malekfar, R., Bellah, S. M. (2019). Effects of energy and hydrogen peroxide concentration on structural and optical properties of CuO nanosheets prepared by pulsed laser ablation. *Results in Physics, 15,* 102610. DOI 10.1016/j.rinp.2019.102610.
35. Jang, H., Lim, S. H., Choi, J. S., Park, Y. (2015). Antibacterial properties of cetyltrimethylammonium bromide-stabilized green silver nanoparticles against methicillin-resistant Staphylococcus aureus. *Archives of Pharmacal Research, 38(10),* 1906–1912. DOI 10.1007/s12272-015-0605-8.
36. Omurzak, E., Tegin, R. A. A., Kyzy, A. B., Satyvaldiev, A., Zhasnakunov, Z. et al. (2018). Effect of surfactant materials to nanoparticles formation under pulsed plasma conditions and their antibacterial properties. *Materials Today: Proceedings, 5(7),* 15686–15695.
37. Abd Zaid, S. M., AbdulRazak, A. A., Abid, M. F. (2022). A review of nano-catalyst applications in kerosene desulfurization techniques. *Journal of Applied Sciences and Nanotechnology, 2(2),* 86–102. DOI 10.53293/jasn.2022.4302.1094.

38. Gupta, A., Mumtaz, S., Li, C. H., Hussain, I., Rotello, V. M. (2019). Combatting antibiotic-resistant bacteria using nanomaterials. *Chemical Society Reviews, 48(2),* 415–427. DOI 10.1039/C7CS00748E.
39. Gabrielyan, L., Trchounian, A. (2019). Antibacterial activities of transient metals nanoparticles and membranous mechanisms of action. *World Journal of Microbiology and Biotechnology, 35(10),* 1–10. DOI 10.1007/s11274-019-2742-6.
40. Lalitha, K., Kalaimurgan, D., Nithya, K., Venkatesan, S., Shivakumar, M. S. (2020). Antibacterial, antifungal and mosquitocidal efficacy of copper nanoparticles synthesized from entomopathogenic nematode: Insect–host relationship of bacteria in secondary metabolites of *Morganella morganii* sp. (PMA1). *Arabian Journal for Science and Engineering, 45(6),* 4489–4501. DOI 10.1007/s13369-020-04487-6.
41. Khademolqorani, S., Banitaba, S. N. (2022). Application of electrosprayed nanoparticles as targeted drug delivery systems: A mini review. *Journal of Applied Sciences and Nanotechnology, 2(2),* 1–7. DOI 10.53293/jasn.2021.4462.1111.